We are IntechOpen, the world's leading publisher of Open Access books
Built by scientists, for scientists

5,800
Open access books available

142,000
International authors and editors

180M
Downloads

Our authors are among the

154
Countries delivered to

TOP 1%
most cited scientists

12.2%
Contributors from top 500 universities

WEB OF SCIENCE™

Selection of our books indexed in the Book Citation Index in Web of Science™ Core Collection (BKCI)

Interested in publishing with us?
Contact book.department@intechopen.com

Numbers displayed above are based on latest data collected.
For more information visit www.intechopen.com

Chapter

Electronic Structure of Chlorophyll Monomers and Oligomers

Juha Matti Linnanto

Abstract

This chapter deals with the electronic structure of chlorophyll molecules and their complexes. Different theoretical and quantum chemical calculation methods are used to study the molecular and electronic structure of chlorophylls. Studied spectral region covers ultraviolet and infrared spectral regions, containing blue side of the Soret band, as also traditional Q_y band region. Thus, there are not only focusing on the traditional Q_y, Q_x, and Soret transitions of chlorophylls but also high-energy transitions (in this region also proteins and nuclei acids absorb light). The aim is to show the effect of molecular conformation on the electronic states and thus on the absorption and emission spectra of monomers and oligomers. In chlorophyll-protein complexes, such conformation effect finetuning the spectral transitions and increases overlap between donor and acceptor states of energy transfer processes. Also, the role of vibronic transition in the shape of absorption and emission spectra of the studied systems will be considered.

Keywords: absorption spectrum, bacteriochlorophyll, B3LYP, CAM-B3LYP, chlorophyll, conformer, exciton theory, fluorescence spectrum, hydrogen bond, light-harvesting antenna, vibronic transition, WSCP, quantum chemistry

1. Introduction

Pigment molecules of light-harvesting (LH) antennae and reaction centers, in most cases noncovalently bound to proteins, are the heart of the photosynthetic apparatus of all photosynthetic prokaryotes and eukaryotes. Pigments differ from one phylum to another, and the relative amounts may vary not only from phylum to phylum and species to species, but even from specimen to specimen. Pigment compositions are different in shade-adapted and sun-adapted leaves of the same tree, in young and old cells, in specimens grown in green light and those grown in red light [1–4]. The chemical structure of a pigment molecule may also change in response to growth conditions [5–10]. An understanding of the structure and photosynthetic properties of pigment molecules is a necessary first step to any understanding of antenna and reaction centers. The primary function of pigment molecules is to absorb a photon of light quantum, and the color of the pigment indicates the wavelengths of light reflected. After absorption processes, pigment molecules of light-harvesting antenna complexes become electronically excited. The excitation is then transferred to a

reaction center, where the excitation energy is transformed into a stable charge separation. And finally, a series of electron and proton transfer and biochemical reactions convert the energy of the Sun's photons into chemical energy in the form of sugars, lipids, and other compounds that sustain cell life [11].

The primary pigments of photosynthesis are chlorophylls (Chls) and bacteriochlorophylls (BChls), they both are cyclic tetrapyrroles. Other photosynthetic pigments, phycobilins (linear tetrapyrroles) and carotenoids (acyclic conjugated hydrocarbons) are often referred to as accessory pigments. There are several types of Chl and BChl molecules (**Figure 1** and **Tables 1** and **2**), but terrestrial plants possess only Chl *a* and Chl *b* molecules. Whereas photosynthetic bacteria possess several types of BChls. For example, BChls *c*, *d*, and *e* are the main pigments of green sulfur bacteria, and BChls *a* and *b* are the main pigments of purple bacteria. In cyanobacteria and in red and

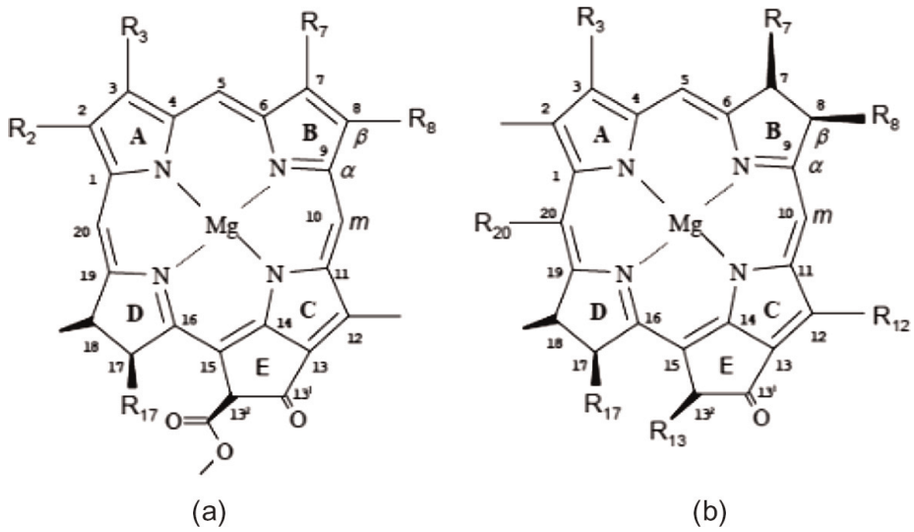

Figure 1.
*General presentation of the chemical structure and IUPAC numbering scheme of chlorophylls (a) and bacteriochlorophylls (b) (see **Tables 1** and **2**).*

Molecule	R_2	R_3	R_7	R_8	R_{17}
Mg-C type[a]					
Chl *a*	$-CH_3$	$-CH=CH_2$	$-CH_3$	$-CH_2-CH_3$	$-CH_2-CH_2-CO-O-R'$[c]
Chl *b*	$-CH_3$	$-CH=CH_2$	$-CHO$	$-CH_2-CH_3$	$-CH_2-CH_2-CO-O-R'$[c]
Chl *d*	$-CH_3$	$-CHO$	$-CH_3$	$-CH_2-CH_3$	$-CH_2-CH_2-CO-O-R'$[c]
Chl *f*	$-CHO$	$-CH=CH_2$	$-CH_3$	$-CH_2-CH_3$	$-CH_2-CH_2-CO-O-R'$[c]
Mg-P type[b]					
Chl c_1	$-CH_3$	$-CH=CH_2$	$-CH_3$	$-CH_2-CH_3$	$-CH=CH-CO-OH$
Chl c_2	$-CH_3$	$-CH=CH_2$	$-CH_3$	$-CH=CH_2$	$-CH=CH-CO-OH$
Chl c_3	$-CH_3$	$-CH=CH_2$	$-CO-O-CH_3$	$-CH=CH_2$	$-CH=CH-CO-OH$

[a]*In the Mg-chlorin type of pigment the C17-C18 bond is a single bond*
[b]*In the Mg-porphyrin type of pigments the C17-C18 bond is a double bond*
[c]*R′ is phytyl*

Table 1.
*Substituents of natural chlorophylls. For basic structure see **Figure 1a**.*

Molecule	R_3	R_7	R_8	R_{12}	R_{13}	R_{17}	R_{20}
Mg-BC type[a]							
BChl *a*	–CO–CH_3	–CH_3	–C_2H_5	–CH_3	–CO–O–CH_3	–C_2H_4–CO–O–R'[c]	–H
BChl *b*	–CO–CH_3	–CH_3	=CH–CH_3	–CH_3	–CO–O–CH_3	–C_2H_4–CO–O–R'[c]	–H
BChl *g*	–CH=CH_2	–CH_3	=CH–CH_3	–CH_3	–CO–O–CH_3	–C_2H_4–CO–O–R'[d]	–H
Mg-C type[b]							
BChl *c*	–CHOH–CH_3	–CH_3	–C_2H_5	–CH_3	–H	–C_2H_4–CO–O–R'[d]	–CH_3
			–C_3H_7	–C_2H_5			
			–C_4H_9				
			–C_5H_{11}				
BChl *d*	–CHOH–CH_3	-CH_3	–C_2H_5	–CH_3	–H	–C_2H_4–CO–O–R'[d]	–H
			–C_3H_7	–C_2H_5			
			–C_4H_9				
			–C_5H_{11}				
BChl *e*	–CHOH–CH_3	–CHO	–C_2H_5	–C_2H_5	–H	–C_2H_4–CO–O–R'[d]	–CH_3
			–C_3H_7				
			–C_4H_9				
			–C_5H_{11}				
BChl *f*	–CHOH–CH_3	–CHO	–C_2H_5	–C_2H_5	–H	–C_2H_4–CO–O–R'[d]	–H

[a]*In the Mg-bacteriochlorin type of pigments the C7-C8 bond is a single bond*
[b]*In the Mg-chlorin type of pigments the C7-C8 bond is a double bond*
[c]*R' is phytyl*
[d]*R' is farnesyl.*

Table 2.
Substituents of the natural bacteriochlorophylls. For basic structure see ***Figure 1b****.*

cryptophyte algae, the main pigments are Chl *a* and phycobilins. Carotenoids have a role in all photosynthetic organisms.

The Chls and BChls are a group of tetrapyrrolic pigments with common structural elements and functions. In chemical terms, they are cyclic tetrapyrroles of the porphyrin, chlorin, or bacteriochlorin oxidation states, which are characterized by a fifth, cyclopentanone ring ortho-perifused (ring E in **Figure 1**) to the pyrrole ring of the porphyrin, chlorin, or bacteriochlorin nucleus with an attached carbonyl ester group and a central Mg atom. Coming from different peripheral substituents, these molecules contain several chiral centers. For natural pigments, the most common are 13^2 and 3^1 epimers [10, 12–14]. For example, the 13^2-epimers of Chl *a* constitute the primary electron donor of Photosystem I of plants and cyanobacteria, and 3^1-epimers of BChl *c*, *d,* and *e* are present in chlorosome antenna elements [10, 13–17]. Conjugated tetrapyrrole ring, a chromophore, allows Chl and BChl molecules to absorb visible light.

The characteristic feature of the ground-state absorption spectrum of monomeric Chls and BChls in organic solvents are the two bands in the long wavelength region 540-850 nm, which have been assigned as transitions to the two lowest singlet excited electronic states. The strong absorption bands in the region 300 to 475 nm are

transitions to higher singlet electronic excited states of Chls and BChls (See **Figure 2**). These absorption bands, as also the corresponding transitions and excited states, are generally referred to as Q_y, Q_x, and B (or B_x, B_y or B_1, B_2 or Soret), in keeping with the nomenclature used for porphyrin in earlier studies [18]. Subscripts x and y indicate transition polarization orientations. In addition, with these characteristic absorption bands, in the ultraviolet spectral region exist two other strong bands at about 260 nm and below 200 nm. There is a correlation between the position of the Q_y band and chemical structure of the conjugated chromophore. Pigments with Mg-bacteriochlorin (Mg-BC) nucleus (BChl *a*, *b,* and *g*) absorb the longest wavelength, and pigments with Mg-porphyrin (Mg-P) nucleus (Chl c_1, c_2, and c_3) absorb the shortest wavelength in the Q_y spectral region (**Figure 2**) [19, 20]. Following the Q_y state energy order found from spectroscopic studies of porphyrin, chlorin, and bacteriochlorin molecules [21, 22]. Also absorption band intensity depends on the chemical structure of the chromophore. The ratio of the absorption maximum of the Soret band to the maximum of the Q_y band is largest for the pigments belong to the Mg-P group [19, 20]. It is typically larger than six for the Mg-P-type pigments, whereas it is less than four for the Mg-chlorin (Mg-C)-type of pigments [19, 20]. For the Mg-BC-type of pigments it is less than one and a half [19, 20]. Additionally, in pigments belong to the Mg-C group (Chl *a*, *b*, *d*, and *f* and BChl *c*, *d*, and *e*) the weak absorbing Q_x state overlaps with the vibronic transition of the lowest singlet excited Q_y state, making an accurate determination of its position in the absorption spectrum of Mg-C-type of (B)Chls difficult [19, 20]. Whereas in BChl *a*, *b*, and *g* molecules, having Mg-BC nucleus, the Q_x band is clearly visible in the spectrum (See **Figure 2**) [19, 20].

Coming from different peripheral substituents, pigments belong to the same chromophore group have different transition energies and shapes of spectra. For example, by considering pigments belong to the Mg-C group. The only difference in the structure of Chl *a* and Chl *b* is substitution at the R_7 position (See **Figure 1**), where Chl *a* has a methyl group and Chl *b* an acetyl group. This small structural difference causes a blue shift of the Q_y absorption from 671 nm in Chl *a* to 655 nm in Chl *b* in pyridine at

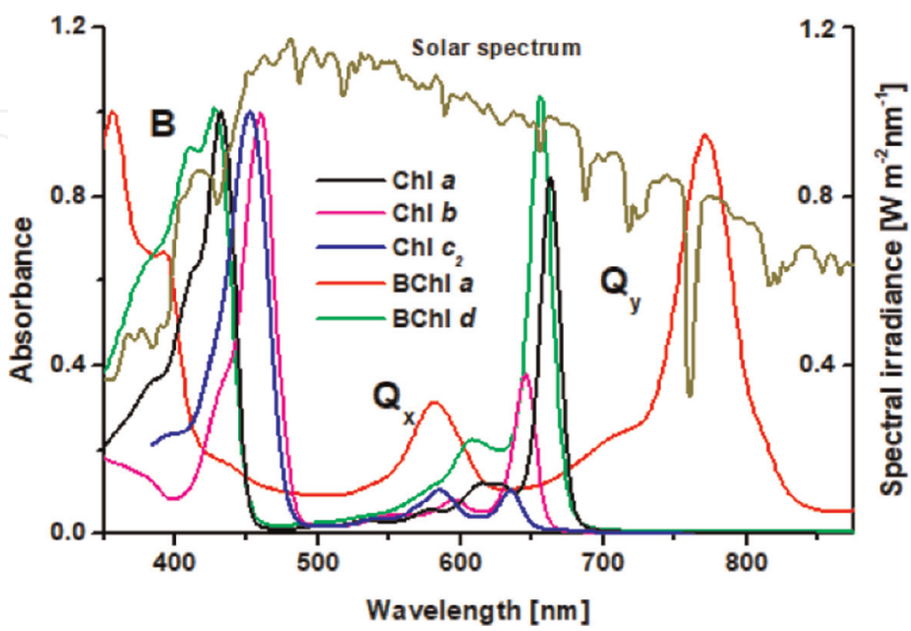

Figure 2.
Ground-state absorption spectra of Chl a, *Chl* b, *Chl* c_2, *BChl* a, *and BChl* d *at room temperature. The main Soret band is scaled to unity. The solar spectrum was obtained from Jari Kemppi, The Finnish Defense Forces.*

room temperature (RT) [19]. Also, Chl *a* has a stronger intensity of the Q_y band than that of Chl *b* as compared to the Soret band. Indicating that peripheral substituents, especially substituents those increase/decrease (perturb) conjugated length of the molecule, affect the electronic structure of chromophore nuclei. Similarly, the only difference in the structures of Chl *a* and Chl *d* or Chl *f* is substitution at the R_3 or R_2 position, respectively. When a vinyl group (Chl *a*) at position R_3 is replaced with an acetyl group (Chl *d*) or a methyl group (Chl *a*) at position R_2 is replaced with an acetyl group (Chl *f*). It causes a redshift of the Q_y absorption from 671 nm (Chl *a*) to 697 nm (Chl *d*) or 706 nm (Chl *f*) in pyridine at RT [19, 23], keeping the intensity ratio between the Soret and Q_y bands almost unchanged. When a vinyl group (Chl *a*) at position R_3 is replaced with a hydroxyethyl group (BChl *d*), a blue shift of the Q_y absorption from 671 nm to 657 nm in pyridine solution at RT is observed [19]. For different homologous structures of BChl *c*, *d,* and *e* molecules having different degrees of methylation at conjugated C_β carbons of the chlorin nucleus at the positions R_8 and R_{12} (see **Table 2** and **Figure 1b**) such significant differences for the spectral shapes and band positions have not been observed. Typically, absorption band positions may vary only a few nm between the homologs [9, 24, 25]. This means that the length of saturated hydrocarbon side chains, at least at the positions R_8 and $R_{12,}$ does not have much effect on electronic structures of the lowest states of the chromophore nuclei. The same is true also for the length of the long hydrocarbon sidechain at the position R_{17}, (B)Chl, and its (bacterio)chlorophyllide derivatives produce almost similar absorption spectrum [26, 27]. These observations might indicate that certain peripheral substituent perturb electron density of the chromophore nuclei and thus causes modification on its spectroscopic properties.

Due to the peripheral substituents and the central Mg atom of (B)Chls, the spectroscopic properties of these molecules are sensitive to the nearest environment around the pigment. Especially the Q_x state has been shown to be very sensitive to the solvent coordination and type of the coordinated ligand [26, 28–30]. Its position may change tens of nm between five and six-coordinated Mg complex structures [26, 30, 31]. Also orientation of peripheral substituents, especially orientations of vinyl and acetyl groups, may have an effect on the transition energies of pigment molecules [32–35]. In a protein environment, coming from different local environments, interactions with nearest amino acids can favor certain orientations of peripheral substituents of (B)Chls. Because of that, the Q_y absorption band of pigment embedded in protein is typically much narrower than that of pigment in organic solution. Thus, the local protein environment can fine-tuning spectroscopic and energy transfer properties of pigment embedded in protein by favoring certain conformers. Also, in protein complexes due to the short inter-pigment distances, exciton couplings between pigment molecules may affect transition energies and transition intensities as compared with the transition energies and transition intensities of isolated pigment molecules [34].

In this work, we create step-by-step the theoretical model for spectral transitions of Chl monomers and Chl oligomers to explain the role of environment, conformers, vibrations, and inter-pigment exciton interactions on the electronic structure of the pigment and pigment complexes. The very first starting model system is an isolated Chl-ligand complex with electronic transitions only. Finally, a more realistic model, Chl oligomer with vibronic transitions is considered. Coming from the fact that the peripheral substituents affect the electronic structure of chromophore, transition energies and transition intensities of different conformers are investigated by using quantum chemical density functional calculation methods. We found out that with the conformer information found from experimental crystal structures and calculated

transition energies and calculated transition dipoles are able to reproduce experimental absorption and emission spectra of several studied systems quite nicely. We were able to explain the unexpectedly high molar extinction coefficient of Chl *b* found in the water-soluble chlorophyll protein as also to explain the large spectral shift found from some LH antenna complexes. Our results suggest that so-called "sergeants and soldier" principle describes H-bond donor and H-bond acceptor interactions in several Chl protein complexes.

2. Electronic structure of pigment molecules

Figure 3a and **b** are shown schematic energy level diagrams (Jablonski diagram) of monomeric and dimeric (B)Chl molecules, respectively. These diagrams illustrate the electronic states of a molecule and the transitions between states. These diagrams are able to explain qualitatively experimentally recorded spectra of the molecule. In **Figure 3a** and **b**, the vibrational ground state of an electronic state is indicated with a thick black line and the higher vibrational states with thinner black lines. There are also shown some phonon states with grey dot lines. For clarity, these phonon states are shown only for a few electronic states [36]. These phonons are vibrations of the environment (protein, solvent, etc.) that are coupled with the electronic states of molecules in condensed matter. **Figure 3b** are also shown some inter-molecular charge transfer (CT) states with dash lines. In monomeric systems, these inter-molecular CT states are forming between monomeric pigment and nearest solvent, etc. molecules, like well-known ligand-metal CT state. Energies of these inter-pigment CT states shown in **Figure 3b** are qualitatively in line with quantum chemical calculation results for strongly coupled BChl *a* oligomers, lowest inter-molecular BChl-BChl CT states appear between the Q_y and Q_x exciton manifolds (the S_1 and S_2 states in **Figure 3b**) [37]. Also, experimental two-photon excitation spectroscopy studies for BChl *a* oligomers have shown states in this spectral region that are not observable in a normal ground state absorption spectroscopy method, because usually, CT states are optically "dark", i.e., one photon-excitation forbidden transitions [38]. Internal conversion (IC) and intersystem crossing (ISC) processes are indicated with grey and light-grey arrows, respectively. IC process occurs when a vibrational state of an electronically excited state is coupled to a vibrational state of a lower electronic state with the same spin multiplicity. Whereas ISC occurs between states with a different spin

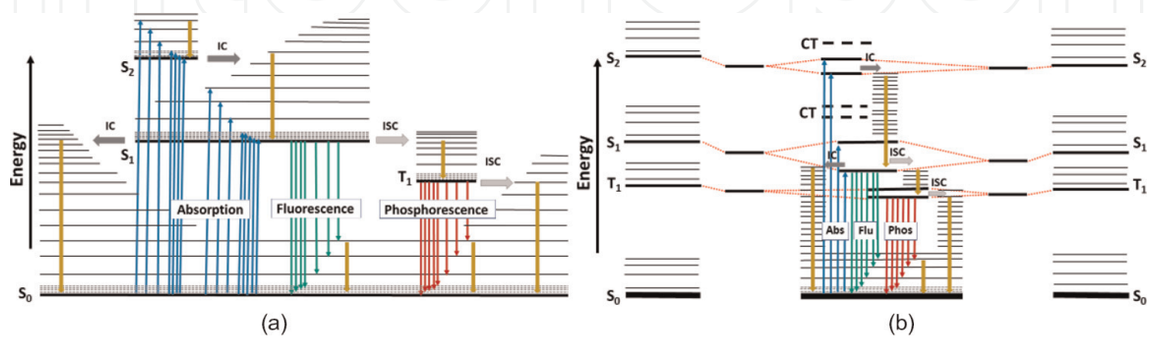

Figure 3.
Scheme of energy levels of monomeric (a) and dimeric (b) (B)Chl complexes. S_0 = electronic ground state, S_{1-2} = singlet excited states, T_1 = triplet excited state, CT = charge transfer state, Abs = absorption, Flu = fluorescence, Phos = phosphorescence, IC = internal conversion, ISC = intersystem crossing. Dark yellow arrows indicate vibration relaxation processes. Red dot lines in the B indicate the effect of environmental shifts and exciton couplings on excited state energies. See the text for details.

multiplicity. These non-radiative relaxation processes are dominant processes in the photophysics of (B)Chls, where the triplet state quantum yield is about 0.20-0.88 and a phosphorescence quantum yield of only about $2*10^{-5}$ or even smaller [23, 39–43]. Dark-yellow arrow indicates vibration relaxation processes. This process involves the dissipation of energy from the molecule to its surrounding. As can be seen in **Figure 3b**, one nondegenerate excited state of a free monomer in dimer corresponds not to one but to two exciton states. This splitting is usually called Davydov splitting [44]. The energy gap between the two states of dimer depends on the exciton coupling strength between the states as also as the energy difference between the coupled electronic excited states of the individual molecules. Transition energy difference, if any, between free identical pigments originates from conformation differences as also from different environmental shifts [45, 46]. In **Figure 3b** was assumed that environmental shift decreases energies of T_1, S_1, and S_2 states. For larger oligomers the excitation energy of the oligomer will split up into as many levels of excited states as is a number of molecules in the oligomer. For crystals, if the unit cell contains *N* identical molecules, then the excitation energy of the crystal will split up into *N* levels of excited states [44].

2.1 Electronic transitions

The origin of the S_1 (Q_y) and S_2 (Q_x) states shown in **Figure 3** is qualitatively explained by the famous Gouterman four orbital model, in which the two highest occupied molecular orbitals (HOMO-1 and HOMO) and the two lowest unoccupied molecular orbitals (LUMO and LUMO+1) form the active molecular orbital space [47, 48]. And spectral transitions (excited states) are described transitions between these active molecular orbitals. The transition from HOMO to LUMO (HOMO→LUMO) and the transition from the second HOMO (HOMO-1) to the second LUMO (LUMO+1) have a transition dipole moment vector parallel with the y-axis, whereas HOMO-1→LUMO and HOMO→LUMO+1 transitions have transition dipole moment vector parallel with the x-axis coming from the symmetry of wavefunctions of (B)Chls. Because of that, the Q_y state (transition) can be expressed by a linear combination of the HOMO→LUMO and HOMO-1→LUMO+1 transitions. Whereas the Q_x state (transition) is expressed by a linear combination of the HOMO-1→LUMO and HOMO→LUMO+1 transitions. This means that spectral transitions (excited states) are not described with a single configuration but with several (two in the four-orbital model) configurations. If only single configuration model is used, then the calculated Q_y transition energy, i.e. energy difference between HOMO and LUMO, is typically much higher than experimental Q_y transition energy. For example, B3LYP/6-31G* SCRF calculations for five coordinated Chl *a* – 2-propanol and BChl *a* – 2-propanol complexes give the molecular orbital energy difference of 2.38 eV and 1.9 eV (see **Figure 4**), respectively. Whereas experimental Q_y transition energy in 2-propanol solution is 1.87 eV and 1.60 eV for Chl *a* and BChl *a*, respectively. Although the single configuration model overestimates an energy gap between HOMO and LUMO it gives the correct energy order of the Q_y state of Chl *a* and BChl *a*. In addition, it has been observed a linear correlation between the Q_y band position and the energy gap between HOMO and LUMO [34, 49]. But, the single configuration model is not able to describe higher electronic excited states correctly.

It appears that the four-orbital model is too reduced to explain high energy excited states and thus to analyze observed spectra in the Soret region. Also, by using larger active molecular orbital space dimensions is able to produce better the Q_y and Q_x

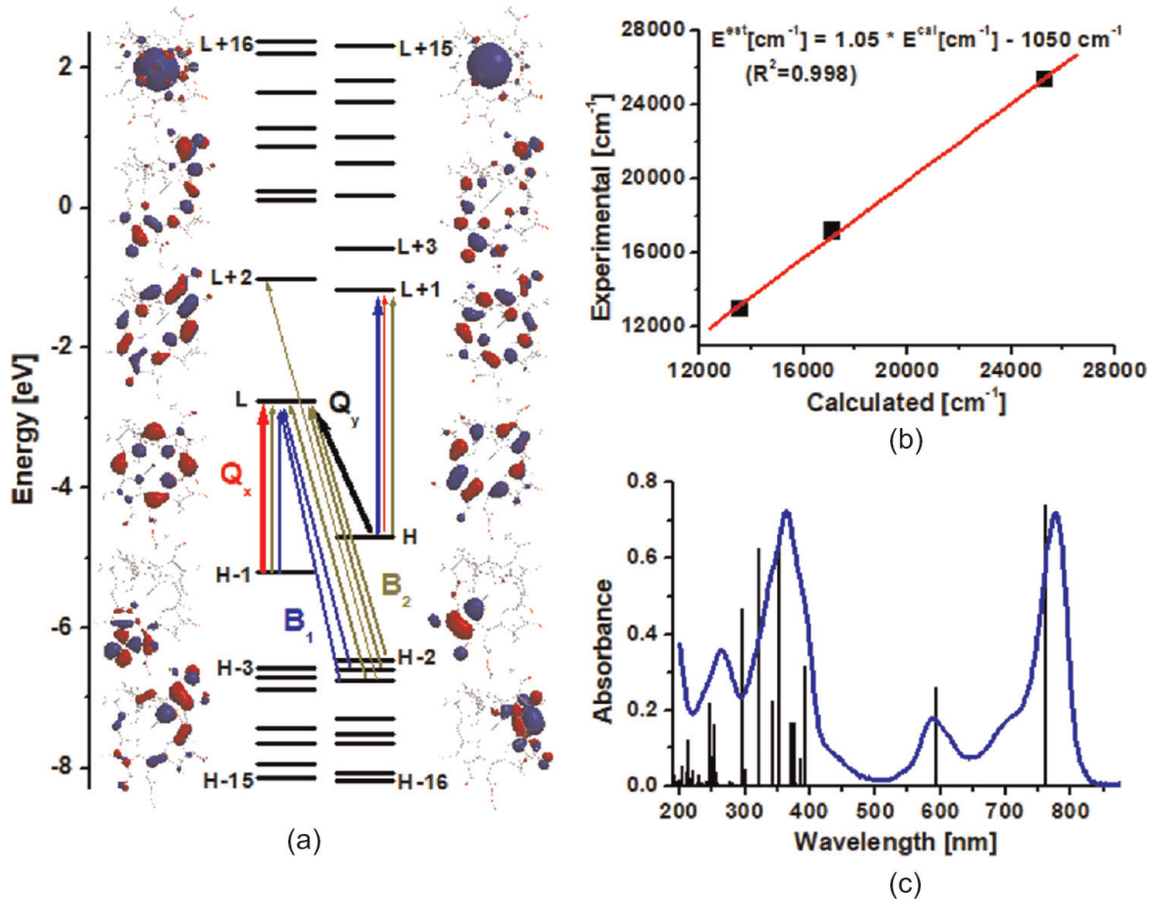

Figure 4.
BChl a *in 2-propanol. (a) Molecular orbital energy level diagram of BChl* a *in 2-propanol with the shapes of six highest HOMO's and six lowest LUMO's. Molecular orbital energies from HOMO-16 (H-16) to LUMO+16 (L+16) are shown. Main configurations of Q_y (black arrow), Q_x (red arrows), B_1 (blue arrows), and B_2 (dark yellow arrows) states/transitions are shown (the thicker arrow is the dominant configuration). In the left-hand side are shown shapes of LUMO+4, LUMO+2, LUMO, HOMO-1, and HOMO-3 (from top to bottom). In the right-hand side are shown shapes of LUMO+5, LUMO+3, LUMO+1, HOMO, HOMO-2, and HOMO-4 (from top to bottom). (b) Linear regression for the Q_y, Q_x, and Soret energies of BChl* a *in 2-propanol. Calculated transition energies are based on TD-B3LYP/6-31G* SCRF method. (c) Experimental and calculated ground-state absorption spectra of BChl* a *in 2-propanol at RT. In the calculated stick spectrum, estimated transition energies are used.*

transition energies [34, 50]. To get a more realistic picture, more than four molecular orbitals are needed to describe the spectral transitions. As an example, in the **Figure 4c** is shown the experimental ground-state absorption spectrum of BChl *a* in 2-propanol at RT with calculated stick spectrum. In the stick spectrum was used estimated transition energies. These energies were got from plots of time-dependent (TD) B3LYP/6-31G* SCRF calculated transition energies of five-coordinated BChl *a* – 2-propanol complex versus experimental solution transition energies (**Figure 4b**) [33, 34, 50–52]. Such linear regression for the Q_y, Q_x, and Soret energies of chromophores has been suggested by Petke *et al.* [53, 54]. In the model structure, 2-propanol was coordinated to the central Mg atom of BChl *a* forming five-coordinated pigment-solvent 1:1 complex structure. This is in line with experimental spectroscopic data, the coordination number of the central Mg atom of (B)Chl *a* in 2-propanol is five [30]. In **Figure 4a** is shown molecular orbitals are needed to explain the shape of the spectrum. These orbitals are localizing mainly on the Mg-BC nuclei. With the arrays are shown main configurations of the four lowest singlet excited electronic states (Q_y, Q_x, B_1, and B_2). The origin of the Q_y and Q_x states (transitions) are in line with the four-orbital model, whereas some main configurations of the B_1 and B_2 states (transitions)

are out of the four-orbital model. As can be seen in **Figure 4a**, it is easy to understand why single configuration model is successful in describing the Q_y energies. The Q_y state has only one main configuration (HOMO→LUMO). Based on the TD-B3LYP result, the B_1 transition has very weak oscillation strength as compared to the Q_y and Q_x transitions of BChl *a*. Whereas the B_2 transition has a large oscillation strength value. As can be seen in **Figure 4c**, there are several spectral transitions that produce the main Soret band. Also, absorption bands in the ultraviolet spectral region at about 260 and 200 nm are composed of several spectral transitions. For the Soret band the main configurations are transitions:

HOMO-8→LUMO, HOMO-3→LUMO, HOMO-2 → LUMO+3, HOMO-1→LUMO+1, HOMO-1→LUMO+2, HOMO→LUMO+1, HOMO→LUMO+3

The band at about 260 nm is due to the main configurations:

HOMO-16→LUMO, HOMO-15→LUMO, HOMO-14→LUMO, HOMO-5→LUMO+1, HOMO-3→LUMO+1, HOMO-3→LUMO+2, HOMO-2→LUMO+1, HOMO-2→LUMO+2, HOMO-1→LUMO+5, HOMO→LUMO+7, HOMO→LUMO+8

And the band at about 200 nm is due to the main configurations:

HOMO-9→LUMO+2, HOMO-9→LUMO+1, HOMO-6→LUMO+3, HOMO-4→LUMO+4, HOMO-4→LUMO+6, HOMO-4→LUMO+7, HOMO-4→LUMO+8,
HOMO-4→LUMO+10, HOMO-3→LUMO+3, HOMO-1→LUMO+10, HOMO→LUMO+11

Calculated electronic transition energies as also transition intensities depend on the calculation method and quality of model structure used [34]. Very often quantum chemical methods overestimate the Q_y, Q_x, and Soret energies. But by using linear regression for transition energies is able to produce spectral shape more-or-less correctly and thus to use calculation/theoretical methods to explain experimentally observed spectroscopic properties of the studied molecule system. In **Figure 5** is shown experimental ground-state absorption spectra of Chl *a* and BChl *a* in 2-propanol at RT with calculated spectra. In calculated spectra, calculated oscillation strengths were spread over Gaussian line shapes (full width at half maximum (fwhm):

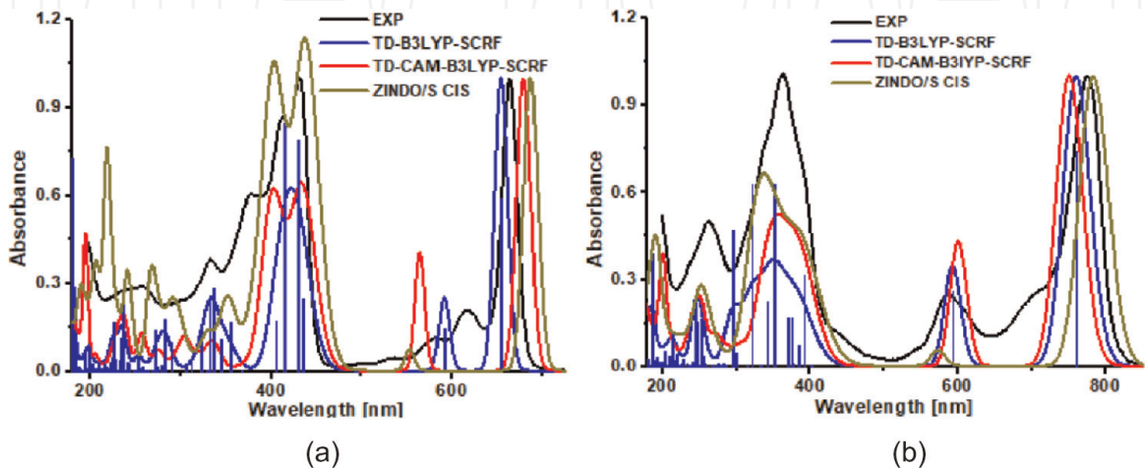

Figure 5
Ground-state absorption spectrum of Chl a *(a) and BChl* a *(b). The main Q_y band is scaled to unity. Deeper information about the spectral bands is shown with the stick spectra base on the TD-B3LYP/6-31G* SCRF results.*

Chl *a* 1700 cm^{-1} in 150–500 nm and 400 cm^{-1} in 500–800 nm; BChl *a* 2500 cm^{-1} in 150–500 nm and 750 cm^{-1} in 500–900 nm). Here are used two different time-dependent density functional calculation methods, TD-B3LYP/6-31G* and TD-CAM-B3LYP/6-31G*, with SCRF solvent model and ZINDO/S CIS semiempirical method to estimate transition energies. In ZINDO/S calculations 75 occupied and 75 unoccupied molecular orbitals were used to form an active space. Calculated model structures were five-coordinated Chl *a* – 2-propanol and BChl *a* – 2-propanol complexes. For the TD-B3LYP and TD-CAM-B3LYP calculations, the model structures were optimized by using B3LYP/6-31G* SCRF and CAM-B3LYP/6-31G* SCRF methods, respectively. But for the ZINDO/S CIS calculations, B3LYP/6-31G* optimized model structures were used, because former calculation studies have been shown that ZINDO/S CIS with B3LYP/6-31G* optimized BChl structures predict transition energies very well [33]. As can be seen, all used methods are able to produce the shape of the spectrum qualitatively. However, they underestimate total absorbance in the high-energy region (200–450 nm). If we will focusing only to the main Soret band (300–500 nm) and the Q (500–850 nm) regions then ZINDO/S CIS overestimates the ratio between integrating intensity (in cm^{-1} units) in the Soret and in the Q regions whereas density functional methods give about one and half times too low value as compared with the experimental ratio. Here must be pointed out, that scattering can affect the measured absorbance, it will appear as a continuous increase in extinction as are going towards shorter wavelengths. Thus, people cannot neglect its role in the high-energy spectral region. As can be observed in **Figure 5a** and **b**, the shape of Soret band is different between Chl *a* and BChl *a* molecules. In the BChl *a* there is a well observable low-energy tail in the experimental spectrum [19, 20], indicating the presence of additional electronic state(s) between the Soret and the Q_x states or presence of impurities. Whereas in Chl *a* such absorbing state seems not to be in present [19, 20]. The calculation methods for the BChl *a* gave excited electronic state with almost zero oscillation strength in this region. Former femtosecond infrared study of monomeric BChl *a* in acetone solution has given evidence for the existence of an electronic state (s) corresponding to one-photon transition(s) around 470 nm in region where the low-energy tail is observed [55]. Also former quantum chemical calculations for different BChl *a* solvent complexes have given dark electronic states between the Soret and the Q_x states [34]. Present TD-CAM-B3LYP/6-31G* calculation for BChl *a* – pyridine complex gave five dark states between the Q_y and Soret states, indicating that amount of the dark states might depend on the chemical structures of the BChl *a* - solvent complexes. A similar tail has been observed also for the other Mg-BC type of BChls, whereas it is lacking in the Mg-P and Mg-C type of (B)Chls [20].

2.2 Effect of conformers on transition energies and transition dipoles

As is known, electronic transition energies may depend on the conformation of pigment. Especially orientation of acetyl group at position R_3 in BChl *a* has been shown to have an effect on the transition energies [34, 35]. Just by analyzing molecular orbitals shown in **Figure 4a**, it can be found out that configurations needed to create the Q_y spectral transition possess atomic orbitals in the acetyl group as also atomic orbitals of conjugated carbons of the ring A (see **Figure 1**). Giving explanation why the acetyl group orientation change modifies spectroscopic properties of the BChl *a*. The peripheral group is bound to the conjugated skeleton of the nuclei. However, less is known about the role of conformation on transition dipoles or transition intensities. In **Figure 6** is shown an effect of vinyl group (bound to the conjugated carbon

C_3 of the ring A, see **Figure 1**) orientation on the Q_y energy and the Q_y transition dipole moment of four-coordinated Chl *a* and *b* molecules by using TD-CAM-B3LYP/6-31G* method. As can be seen, the orientation of the peripheral group has a strong effect both on the transition energy and on the transition dipole moment. This means that the electronic structure of molecule is much more complex than the schematic energy level diagrams shown in **Figure 3**. In real picture, the horizontal energy levels in **Figure 3** are multidimensional Born-Oppenheimer energy surfaces. With **Figure 6** is easy to understand that if the conformation of pigment embedded in protein is totally different than conformers dominate in solution, then not only spectral band positions but also band intensities may differ a lot between these two different systems. Also, coming from this different conformation distribution between pigments in protein and in solvent environments, the width of the Q_y absorption band of the (B) Chl embedded in protein is typically narrower than the band of pigment in the solution.

There are discussions about the origin of unexpectedly high molar extinction coefficient of Chl *b* embedded in the water-soluble chlorophyll protein (WSCP) when compared with the corresponding Chl *a*-reconstituted complexes [56, 57]. Molar extinction coefficient of Chl *b* molecule in the Q_y region is about 20–30% larger in the WSCP system than that of Chl *b* in ethanol solution. For Chl *a* molecule embedded in the WSCP the value is 11% less or equal to the value in Chl *a* - ethanol solution. Because of the well-known quadratic relation between the transition dipole moment and the molar extinction coefficient, the change of the molar extinction coefficient of Chl *b* could be explained by analyzing orientations of peripheral functional groups of Chl *b* conformers found from the X-ray structure of Chl *b*-WSCP protein, at least in

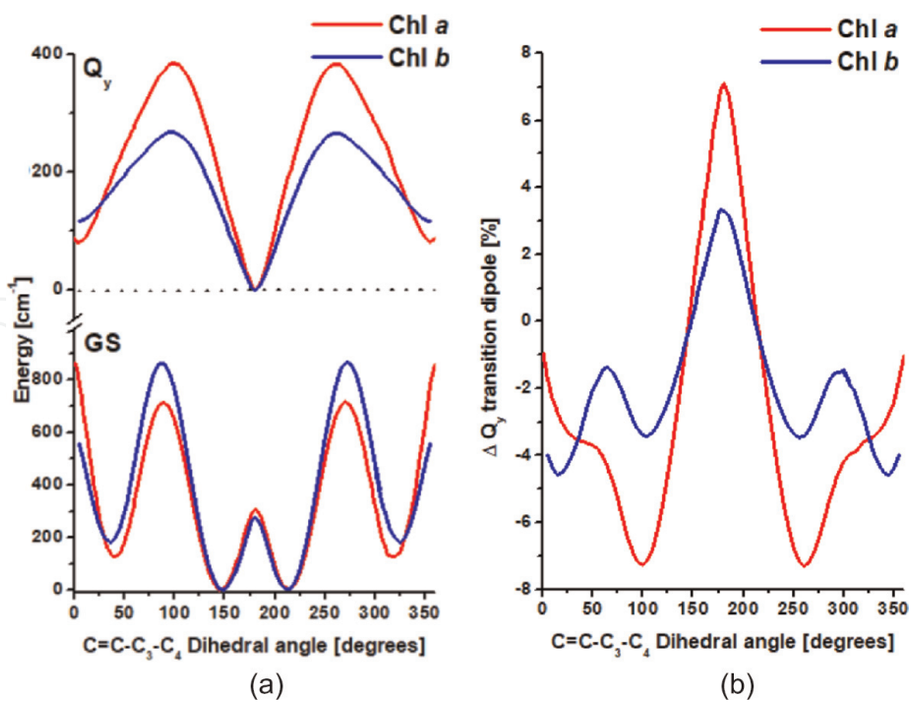

Figure 6.
(a) Dependence of the electronic ground-state (GS) and Q_y excited-state energy on the 3-vinyl group dihedral angle in four-coordinated Chl a *and Chl* b *monomers. Energies are compared to the minimum energy of the electronic ground state and to the first singlet excited electronic state (minimum energy is set to 0 cm^{-1}). (b) Dependence of the magnitude of the Q_y transition dipole moment on the 3-vinyl group dihedral angle in the four-coordinated Chl* a *and Chl* b *monomers as compared to the value of the minimum energy structure of the electronic ground state. TD-CAM-B3LYP/6-31G* method is used in calculations.*

the lowest level of approximation. For the Chl *b* molecules of the WSCP protein (WSCP has four Chl *b* molecules) are found dihedral angle values of the vinyl group at about 15, 194, 198, and 204 degrees [56]. These give change of the Q_y transition dipole moments of about -4.7%, 2.3%, 2.5%, and 0.8%, respectively, as compared with the values of the minimum energy structure (see **Figure 6b**). To taking account also orientation differences of acetyl (R_7) and ethyl (R_8) groups, the change of the Q_y transition dipole moments are then -2.3%, 2.0%, 3.6%, and 4.5%. For five-coordinated structures with dihedral angle values found from the X-ray structures, corresponding values are: -2.7%, 9.5%, 5.9%, and 9.5%, respectively. This result can explain qualitatively the high molar extinction coefficient value observed for the Q_y transition of the Chl *b*-WSCP protein. Also, ground-state energies of these conformers are so high, that based on Boltzmann distribution they are not dominant conformers at RT. Thus, their impact on the molar extinction coefficient value for the Chl *b* in solution at RT is small. To find out the role of conformers on transition intensities of the Chl *b*-WSCP protein, exciton calculation with conformer corrected transition dipole couplings are needed [58, 59]. Coming from large inter-Chl distances in the WSCP protein (the shortest Mg-Mg distance is about 9.6 Å), a dipole-dipole approximation can be used to calculate exciton couplings in this system. Present exciton calculation with the conformer-corrected Q_y transition dipole moment values (-2.7%, 9.5%, 5.9%, and 9.5%), the corresponding Q_y transition energies, and the X-ray structure information produces about 12 % larger oscillation strength value in the Q_y spectral region as compared with the calculation having only identical conformers (optimized ground state geometry structure). This value is roughly 50% of the experimentally observed increase of the Q_y intensity. Thus, this reduced structure model and TD-CAM-B3LYP method are able to suggest that conformation difference could be the main origin of the huge increase of the molar extinction coefficient found from the Q_y spectral region of the Chl *b*-WSCP proteins.

Conformation difference could also explain a huge spectral shift (50 nm) found from the LH2 and LH3 antenna complexes of purple bacterium *Rhodopseudomonas acidophila* [60, 61]. Based on the X-ray structures of these complexes, there are two different sets of pigments with the dihedral angle of the acetyl group of about -24 and 16 degrees (B850 pigments of the LH2 complex) and of about -30 and -36 degrees (B820 pigments of the LH3 complex). In our previous study has been shown the dependence of the Q_y transition energy on the acetyl group orientation of BChl *a* molecule (see **Figure 6b** in Ref. [35]). With this result is able to estimate that the two different B850 pigment sets have about 170 and 75 cm^{-1} larger Q_y transition energies than that of the optimized BChl *a* molecule. For the B820 pigments, the corresponding values are even larger, about 430 and 320 cm^{-1}. TD-CAM-B3LYP/6-31G* calculated change of Q_y transition dipole moment values are about -3% and -1% for the B850 pigments and about -6% and -4.5% for the B820 pigments as compared to the transition dipole moment of the optimized structure. Exciton calculations with these Q_y transition dipole moment values, Q_y transition energies, and experimental X-ray structures produce half of the experimentally observed band shift and show that in the LH3 antenna the energy difference between the highest and lowest Q_y exciton state (Davidov splitting) is about 12 % smaller than the energy difference in the LH2 complex. Based on experimental fluorescence anisotropy studies, it has been shown that the LH3 complex has about 11% smaller width of the B820 exciton manifold than that of the LH2 complex [62]. Indicating that such reduce model is able to give qualitative results. The too weak calculated shift is coming from the too reduced exciton model used. Dipole-dipole approximation is not good enough to describe

exciton couplings between pigments with van der Walls contact (there are mixing of wavefunctions of adjacent pigments), more better is to use so-called supermolecule approximation [58].

In similar way, different conformers can be used to explain qualitatively the unusual Q_y absorption band red-shift found from different LH1 antenna complexes of the thermophilic bacterium *Thermochromatium tepidum* [63]. In the Ca-bound LH1 complex the Q_y absorption band appears much lower in energy than that in the Ba- or Sr-bound LH1 complexes (915 nm vs. 888 nm at RT, difference 330 cm^{-1}). Based on the experimental X-ray structures, the dihedral angles of the acetyl group of BChl molecules vary in range of |0–5|, |0–37|, and |2–54| degrees in Ca-, Ba-, and Sr- bound LH1 complexes, respectively [63, 64]. Coming from the TD-CAM-B3LYP/6-31G* results [35], BChls with the dihedral angle of acetyl group in range |0–5| degrees have much smaller Q_y transition energies than the pigments with larger dihedral angle value. For example, the Q_y transition energies of pigments with the angle of |0–5| degrees are approximately about 200 or 400 cm^{-1} smaller than that for the pigment with the angle of 20 or 30 degrees, respectively. TD-CAM-B3LYP/6-31G* calculations indicate also that the Q_y transition dipole moment is larger for the pigments with the angle of |0–5| degrees than for the two other sets of the pigments, suggesting that the exciton couplings are the strongest in the Ca-bound LH1 complex. Thus, conformer analyze predicts that the Q_y absorption band of the Ca-bound LH1 complex appears in lower energy than that of the Ba- and Sr-bound LH1 complexes. Very often this kind of the Q_y band shifting processes are explained with the H-bond or with the breaking of H-bond systems [65]. TD-CAM-B3LYP/6-31G* calculations for the identical BChl *a* conformers (the B850 BChl *a* from LH2 antenna of *Rhodopseudomonas acidophila*) [61] with and without explicit H-bond donor ligand (tryptophan) indicate that the "additional" H-bond effect could decrease the Q_y transition energy of about 200 cm^{-1}. This energy value depends on the type of the H-bond donor as also from the distance between H-bond donor and acceptor residues, of course. This additional H-bond or surrounding effect is actually in line with experimental observations, those show that Chls in gas phase have larger Q_y transition energy than Chls in solution [66, 67]. In addition, calculations for the BChl *a* complexes where the position of the H-bond donor was changed indicate that the orientation of the acetyl group (H-bond acceptor) follows the position of the donor. There were H-bond complexes with a large variation of the dihedral angle of the acetyl group from 0 to a few tens of degrees. Thus, the H-bond itself (i.e. non-zero electron density between H-bond donor and acceptor ligands) is not the reason for the observed huge band shifts, but the acetyl group orientation has the main role in the band-shifting processes. This is in line with absorption spectra of (B)Chl monomers in different nonpolar and polar solvent environments, although there are H-bonds complexes a huge Q_y band shift is not observed [30]. Thus, the role of the H-bond donor is like the "sergeants and soldiers" principle, orientation of the acetyl group (H-bond acceptor) arises from a "sergeants and soldier" effect i.e. from the position of the H-bond donor around the acceptor.

To get the more exact picture about the role of conformer on exciton energies and transition intensities of pigment-protein complexes, higher resolution X-ray structures are needed. In addition, as is known, mixing between different exciton states might borrow intensity [68]. Thus, the exciton model with couplings between the Q_y and other excited states of pigment might give additional information about studied systems. Also, here was used quite reduced model structure, containing only pigment with one ligand, lacking the main part of the nearest protein environment. Thus, chromophore ring distortions observed in the crystal structures of pigment-protein

complexes were not involved in the calculations, because of geometry optimization. Such distortions have been shown to have effect on transition energies [69].

2.3 Vibronic transitions

As is seen in **Figure 5** the shape of the calculated Q_y absorption band differs from the experimental band shape. The reason is lacking vibration levels, i.e. calculations were done without vibronic transitions. As can be found in **Figures 3** and **7**, vibronic transitions are able to produce transition intensities in the high-energy side of the Q_y absorption band as also in the low-energy side of the emission band [70–72]. This is well observed in **Figure 7a**, there are number of vibration levels in the high energy side of the Q_y band that can be the final states of the absorption process. Similarly, in the emission process, there are lot of vibration states above the vibration ground state of the electronic ground states those can be the final states of emission transitions as is well observed from **Figure 7c**. In **Figure 7c** is shown experimental fluorescence and difference fluorescence line narrowing (ΔFLN) [73] spectra of Chl *a* in 1-propanol at 4.5 K. Shortly speaking, in the ΔFLN method is used a narrow-band laser excitation to select spectrally identical group of pigments (conformers) to eliminate inhomogeneous broadening of the spectral band [74]. The ΔFLN spectrum shows a strong purely electronic line at 0 cm^{-1} (so-called zero-phonon line. It originates from the transition between vibration ground states of the Q_y state and the electronic ground state. This 0-0 transition is shown in the left-hand side of **Figure 7a**). It appears along with a broad and asymmetric phonon wing or phonon sideband peaking at

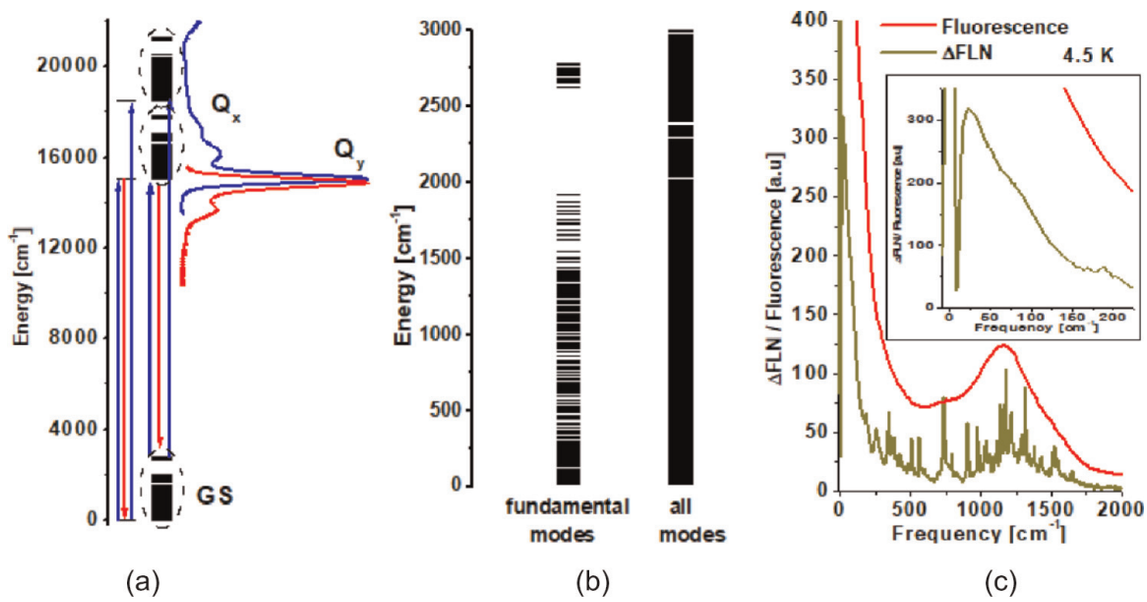

Figure 7.
(a) Energy level diagram of Chl a *with and without vibrational states. In the left-hand side is shown only pure electronic states and in the right-hand side is shown also calculated vibrational states. Here is also shown experimental ground-state absorption and fluorescence spectra of Chl* a *in 1-propanol at RT. Absorption and fluorescence are indicated with blue and red arrows, respectively. Black circles indicate vibration manifolds (For clarity, only fundamental modes are shown). (b) Distribution in the energy of the vibrational modes in the ground electronic state of Chl* a *molecule. In the left-hand side is shown all fundamental modes and fundamentals with their 20 overtone modes that have energy below 3000 cm^{-1} are shown in the right-hand side. Vibration states are calculated by using semiempirical PM6 method. (c) Experimental low-temperature fluorescence and difference fluorescence line narrowing spectra of Chl* a *in 1-propanol. Inset of panel C shows the shape of phonon band. For clarity, only part of the spectrum is shown. See text for further explanations.*

about 20 cm^{-1} (see inset of **Figure 7c**) as well as several distinct vibrational bands. The general shape of the ΔFLN spectrum overlaps nicely with the shape of the inhomogeneously broadened fluorescence spectrum of Chl *a* in 1-propanol at 4.5 K. Vibration modes shown in **Figure 7** are calculated with the semiempirical PM6 method. The fundamental mode energies are well in range of energies found from infra-red absorption spectra of Chl *a* [75]. Infra-red spectra show bands around 2800 cm^{-1} and below 1800 cm^{-1}. When also overtones of modes are considered, continuum of the states are observed (**Figure 7b**). This indicates that overtones of modes as also combination of modes have role in the IC and ISC processes shown in **Figure 3**, because the energy gap between the electronic states could be much larger than the energy of the highest fundamental mode of vibration. It has been also suggested that overtones of modes could increase energy transfer efficiency, coming from the fact that with these transitions overlap between absorbing and fluorescing states will increase [71]. Based on experimental fluorescence studies, extra-long fluorescence tails of Chl *a* and BChl *a* molecules have been observed as far as 4000 cm^{-1} from the main Q_y band [71]. At high temperatures, when vibration excited states of the electronic ground state are populated, vibronic transitions from the thermally populated hot vibration states of the ground electronic state can produce absorbance also far in low-energy side of the absorption band. For example, a weak absorption tail has been observed as far as 2400 cm^{-1} from the absorption peak in the low-energy side of the Q_y band for Chl *a* and BChl *a* molecules at RT [35, 76]. The shape of these tails was able to explain by using vibronic transitions, mainly with the overtones of modes. Also, vibronic transitions or better strong vibronic coupling between Q_y and Q_x states, have been shown to have role in the position of the Q_x absorption band of Chl *a* molecule in different solvents [77]. With this information, the Q_x state shown in **Figure 7a** is coupled with some high energy vibrations of the Q_y state and thus the Q_x transition give intensity also in a region where to appear the Q_y state vibrations.

To calculate normal modes of vibrations optimized geometries are needed. This limits the size of the model system used. Very often model system contains only a single pigment or pigment with one ligand molecule coordinated to the central Mg atom [35, 70–72, 76–79]. Such models are far away from realistic model structure for a pigment in real solvent or protein environment. These calculations forget a real conformer of the pigment and the nearest environment around it. In some case is able to use experimental ΔFLN spectrum to estimate Franck-Condon (FC) coefficients of vibrations needed in vibronic calculations. This kind of estimated set of FC coefficients describes a system only at low temperature, there are lacking transitions (FC coefficients) from thermally populated hot vibration states those are essentials at higher physiological temperatures. In **Figure 8** are shown experimental and calculated absorption and non-line narrowed fluorescence spectra of Chl *a*-WSCP protein at 4.5 K [80]. To obtain realistic shapes of the spectra, the stick exciton spectra were dressed with Gaussian homogeneous band shapes (fwhm) of 120 cm^{-1} (fluorescence) and 150 cm^{-1} (absorption). In the calculations were used vibronic exciton model [79]. The FC coefficients, i.e. overlap integrals between the vibration wavefunctions of the electronic ground state and the Q_y state, were estimated from the ΔFLN spectrum of Chl *a* in 1-propanol at 4.5 K shown in **Figure 7c** [70]. Here was made such kind of approximations that absorption and fluorescence transitions have identical FC coefficients and that all vibration peaks of the ΔFLN spectrum are coming from the fundamental modes of vibrations. Now each peak position gives the energy of the corresponding fundamental mode (i.e. energy level of vibrations, see **Figure 3**) and a height of peak gives the value of the FC coefficient. In the exciton calculation, the FC coefficients

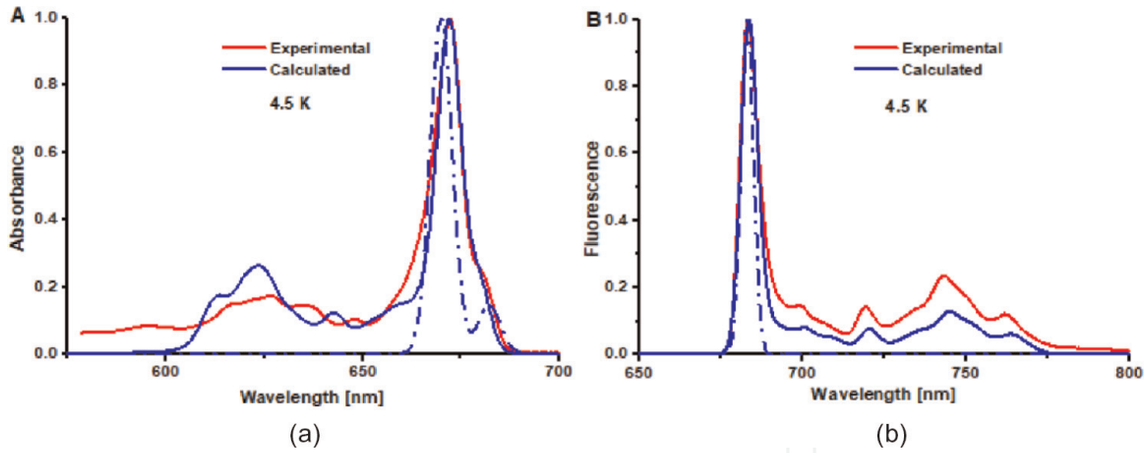

Figure 8.
Calculated and experimental 4.5 K absorption (a) and nonline-narrowed fluorescence (b) spectra of Chl a*-WSCP complex. The solid blue line shows calculated spectra with vibronic transitions and dash-dot blue line shows calculated spectra without vibration levels. The main Q_y band is scaled to unity. See the text for details.*

modulate the magnitude of the electronic transition dipole moment vectors, and thus exciton coupling strengths between the Chl *a* molecules of the WSCP protein. Exciton calculation contains zero phonon line, phonon sideband function, 50 strongest vibration peaks found from the experimental ΔFLN spectrum, conformer corrected Q_y transition energies (0–0 transition), conformer corrected Q_y transition dipoles (+4.5% and +2.3%), and experimental X-ray structure information of Chl *a*-WSCP protein (dihedral angle of the vinyl group: 199.5 and 190.8 degrees. The WSCP has two symmetrical Chl *a* dimers) [81]. With the calculated vibronic exciton spectra are shown also calculated spectra without vibrations (pure electronic exciton model, blue dash-dot line). To compare these two different calculated spectra can be easily found out the role of vibrations in the shape of spectra. Also, as can be seen, because the FC coefficients modulate exciton coupling strengths, absorption band positions and energy gap between the bands (Davidov splitting) are different in these spectra (exciton calculation without vibration levels gives two well separated absorption bands and the gap between these bands are larger than that of the spectrum calculated with the vibronic transitions). At higher temperatures with thermally populated hot vibration states (different sets of FC coefficients), these differences could be even larger. This indicates that exciton couplings estimated from experimental spectra (contains vibrations) could be smaller than that of calculated by using quantum chemical methods (pure electronic states). If the shape of the main absorption band is considered, especially the low-energy side of the band, then we can find out that conformer corrected exciton parameters produce quite nicely the exciton energies of the WSCP protein. The lowest Q_y exciton state gives a weak shoulder in the red side of the band and the other exciton state produces the main band, producing the correct shape of the main Q_y band. To compare with the experimental and the calculated vibronic spectra we can find out that the general shape of the spectrum is well produced. However, some vibronic transitions in the absorption spectrum have too strong intensity (in the experimental spectrum there might appear also Q_x band(s) in this spectral region). And, in the fluorescence spectrum, the 0-0 transition has too dominant role. This result indicates that the used set of the FC coefficients, got from the fluorescence process of Chl *a* in 1-propanol complex, are not good enough to describe the absorption spectrum of Chl *a*-WSCP protein complex perfectly, but still good enough to describe qualitatively shape of both spectra of the complex. Thus, as

the main result of this whole work, it seems that this kind of calculation allows to produce more-or-less correctly the shape of absorption and fluorescence spectra of the pigment-protein complex.

3. Conclusions

Modern quantum chemical methods are able to explain the spectroscopic properties of chlorophylls and their complexes. Very often these methods overestimate transition energies, but the linear regression method is able to estimate transition energies and to produce more or less correct shapes of spectra. This allows to use calculated spectra together with experimental data to get more detailed picture/information about the studied system.

Spectroscopic properties of monomeric and oligomeric chlorophyll complexes depend strongly on the nearest environment around the molecule. The environment can modulate spectral transition energies and transition intensities and can favor certain conformers. Especially orientation of the H-bond acceptor group of pigment molecule arises from the position of the H-bond donor around it. Because different conformers might have totally different physicochemical properties, environment perturbation as fine-tuning spectroscopic and energy transfer properties of pigment oligomers. This work suggests that the orientation of certain functional groups of (bacterio)chlorophylls might have dominant role in pigment-protein complexes.

To produce calculated spectral band shape correctly vibronic transition are needed. With these vibronic transitions are able to study temperature dependence processes and to create more realistic light-harvesting and energy transfer model systems.

This work demonstrates that it is a possible to create a theoretical calculation model/tool, conformer corrected vibronic exciton method, where calculated transition energy and transition dipole moment data are used as parameters to generate input parameters needed in exciton calculations.

Acknowledgements

This research was supported by Estonian Research Council, grant number PSG264.

I would like to thank Prof. Dr. Margus Rätsep and Prof. Dr. Jörg Pieper for giving me the experimental data.

Appendices and nomenclature

Chl	chlorophyll
CT	charge transfer
BChl	bacteriochlorophyll
FC	Franck-Condon
Fwhm	full width at half maximum
HOMO	highest occupied molecular orbital
H-bond	hydrogen bond
IC	internal conversion
ISC	intersystem crossing
LH	light-harvesting

LUMO	lowest unoccupied molecular orbital
Mg-BC	Mg-bacteriochlorin
Mg-C	Mg-chlorin
Mg-P	Mg-porphyrin
RT	room temperature
TD	time-dependent
WSCP	water-soluble chlorophyll protein
ΔFLN	difference fluorescence line narrowing

IntechOpen

IntechOpen

Author details

Juha Matti Linnanto
University of Tartu Institute of Physics, Tartu, Estonia

*Address all correspondence to: Juha.m.linnanto@gmail.com

IntechOpen

© 2022 The Author(s). Licensee IntechOpen. This chapter is distributed under the terms of the Creative Commons Attribution License (http://creativecommons.org/licenses/by/3.0), which permits unrestricted use, distribution, and reproduction in any medium, provided the original work is properly cited.

References

[1] Rabinowitch EG. Photosynthesis. New York: John Wiley & Sons INC; 1969

[2] Yokono M, Murakami A, Akimoto S. Excitation energy transfer between photosystem II and photosystem I in red algae: Large amounts of phycobilisome enhance spillover. Biochimica et Biophysica Acta. 2011;**1807**:847-853. DOI: 10.1016/j.bbabio.2011.03.014

[3] Melis A, Murakami A, Nemson JA, Aizawa K, Ohki K, Fujita Y. Chromatic regulation in *Chlamydomonas reinhardtii* alters photosystem stoichiometry and improves the quantum efficiency of photosynthesis. Photosynthesis Research. 1996;**47**:253-265. DOI: 10.1007/BF02184286

[4] Lichtenthaler HK, Buschmann C, Doll M, Fietz H-J, Bach T, Kozel U, et al. Photosynthetic activity, chloroplast ultrastructure, and leaf characteristics of hight-light and low-light plants and of sun and shade leaves. Photosynthesis Research. 1981;**2**:115-141. DOI: 10.1007/BF00028752

[5] Huster MS, Smith KM. Biosynthetic studies of substituent homologation in bacteriochlorophylls *c* and *d*. The Biochemist. 1990;**29**:4348-4355. DOI: 10.1021/bi00470a013

[6] Borrego CM, Garcia-Gil LJ. Rearrangement of light harvesting bacteriochlorophyll homologues as a response of green sulfur bacteria to low light intensities. Photosynthesis Research. 1995;**45**:21-30. DOI: 10.1007/BF00032232

[7] Borrego CM, Gerola PD, Miller M, Cox RP. Light intensity effects on pigment composition and organisation in the green sulfur bacterium *Chlorobium tepidum*. Photosynthesis Research. 1999; **59**:159-166. DOI: 10.1023/A:1006161302838

[8] Gardiner AT, Cogdell RJ, Takaichi S. The effect of growth conditions on the light-harvesting apparatus in Rhodopseudomonas acidophila. Photosynthesis Research. 1993;**38**: 159-167. DOI: 10.1007/BF00146415

[9] Borrego CM, Garcia-Gil LJ. Separation of bacteriochlorophyll homologues from green photosynthetic sulfur bacteria by reversed-phase HPLC. Photosynthesis Research. 1994;**41**: 157-163. DOI: 10.1007/BF02184156

[10] Ishii T, Kimura M, Yamamoto T, Kirihata M, Uehara K. The effects of epimerization at the 3^1-position of bacteriochlorophylls c on the aggregation in chlorosomes of green sulfur bacteria. Control of the ratio of 3^1 epimers by light intensity. Photochemistry and Photobiology. 2000; **71**:567-573

[11] Ke B. An overview. In: Govindjee, editor. Photosynthesis Photobiochemistry and Photobiophysics. Dordrecht: Kluwer Academic Press; 2001. pp. 1-41. DOI: 10.1007/0-306-48136-7_1

[12] Amesz J. New trends in photobiology: The heliobacteria, a new group of photosynthetic bacteria. Journal of Photochemistry and Photobiology. B. 1995;**30**:89-96. DOI: 10.1016/1011-1344(95)07207-I

[13] Jordan P, Fromme P, Witt HT, Klukas O, Saenger W. Three-dimensional structure of cyanobacterial photosystem I at 2.5 Å resolution. Nature. 2001;**411**: 909-917. DOI: 10.1038/35082000

[14] Bobe FW, Pfennig N, Swanson KL, Smith KM. Red shift of absorption

maxima in chlorobiineae through enzymic methylation of their antenna bacteriochlorophylls. The Biochemist. 1990;**29**:4340-4348. DOI: 10.1021/bi00470a012

[15] Webber AN, Lubitz W. P700: The primary electron donor of photosystem I. Biochimica et Biophysica Acta. 2001; **1507**:61-79. DOI: 10.1016/S0005-2728(01)00198-0

[16] Steensgaard DB, Wackerbarth H, Hildebrandt P, Holzwarth AR. Diastereoselective control of bacteriochlorophyll e aggregation. 3^1-S-Bchl *e* is essential for the formation of chlorosome-like aggregates. The Journal of Physical Chemistry. B. 2000;**104**: 10379-10386. DOI: 10.1021/jp0013356

[17] Olson JM. Chlorophyll organization and function in green photosynthetic bacteria. Photochemistry and Photobiology. 1998;**67**:61-75

[18] Gouterman M. Study of the effects of subctitution on the absorption spectra of porphin. The Journal of Chemical Physics. 1959;**30**:1139-1161

[19] Niedzwiedzki DM, Blankenship RE. Singlet and triplet excited state properties of natural chlorophylls and bacteriochlorophylls. Photosynthesis Research. 2010;**106**:227-238. DOI: DOI/10.1007/s11120-010-9598-9

[20] Taniguchi M, Lindsey JS. Absorption and fluorescence spectra database of chlorophylls and analogues. Photochemistry and Photobiology. 2021; **97**:136-165. DOI: 10.1111/php.13319

[21] Eisner U, Linstead RP. Chlorophyll and related substances. Part II. The dehydrogenation of chlorin to porphin and the number of extra hydrogen atoms in the chlorins. Journal of Chemical Society. 1955:3749-3754

[22] Seely GR. Molecular orbital study of the porphyrins. The Journal of Chemical Physics. 1957;**27**:125-133. DOI: 10.1063/1.1743651

[23] Niedzwiedzki DM, Liu H, Chen M, Blankenship RE. Excited state properties of chlorophyll *f* in organic solvents at ambient and cryogenic temperatures. Photosynthesis Research. 2014;**121**: 25-34. DOI: DOI/10.1007/s11120-014-9981-z

[24] Airs RL, Borrego CM, Garcia-Gil J, Keely BJ. Identification of the bacteriochlorophyll homologues of *Chlorobium phaeobacteroides* strain UdG6053 grown at low light intensity. Photosynthesis Research. 2001;**70**: 221-230. DOI: DOI/10.1023/A:1015146304441

[25] Mizoguchi T, Harada J, Tsukatani Y, Tamiaki H. Isolation and characterization of a new bacteriochlorophyll-c bearing a neopentyl substituent at the 8-positon from the *bciD*-deletion mutant of the brown-colored green sulfur bacterium *Chlorobaculum limna*eum. Photosynthesis Research. 2014;**121**:3-12. DOI: DOI/10.1007/s11120-014-9977-8

[26] Fiedor L, Kania A, Mysliwa-Kurdziel B, Orzel L, Stochel G. Understanding chlorophylls: Central magnesium ion and phytyl as structural determinants. Biochimica et Biophysica Acta. 2008; **1777**:1491-1500. DOI: 10.1016/j.bbabio.2008.09.005

[27] Bruce DL, Duff DCB, Antia NJ. The identification of two antibacterial products of the marine planktonic alga *Isochyrysis galbana*. Journal of General Microbiology. 1967;**48**:293-298

[28] Callahan PM, Cotton TM. Assignment of bacteriochlorophyll *a* ligation state from absorption and

resonance raman spectra. Journal of the American Chemical Society. 1987;**109**: 7001-7007. DOI: 10.1021/ja00257a016

[29] Shipman LL, Cotton TM, Norris JR, Katz JJ. An analysis of the visible absorption spectrum of chlorophyll a monomer, dimer, and oligomers in solution. Journal of the American Chemical Society. 1976;**98**:8222-8230. DOI: 10.1021/ja00441a056

[30] Limantara L, Sakamoto S, Koyama Y, Nagae H. Effects of nonpolar and polar solvents on the Q_x and Q_y energies of bacteriochlorophyll *a* and bacteriopheophytin *a*. Photochemistry and Photobiology. 1997;**65**:330-337. DOI: 10.1111/j.1751-1097.tb08566.x

[31] Evans TA, Katz JJ. Evidence for 5- and 6-coordinated magnesium in bacteriochlorophyll *a* from visible absorption spectrum. Biochimica et Biophysica Acta. 1975;**396**:414-426. DOI: 10.1016/0005-2728(75)90147-4

[32] Gudowska-Nowak E, Newton MD, Fajer J. Conformational and environmental effects on bacteriochlorophyll optical spectra: Correlations of calculated spectra with structural results. The Journal of Physical Chemistry. 1990;**94**:5795-5801. DOI: 10.1021/j100378a036

[33] Linnanto J, Korppi-Tommola J. Structural and spectroscopic properties of Mg-bacteriochlorin and methyl bacteriochlorophyllides *a*, *b*, *g*, and *h* studied by semiempirical, ab initio, and density functional molecular orbital methods. The Journal of Physical Chemistry. A. 2004;**108**:5872-5882. DOI: 10.1021/jp0309771

[34] Linnanto J, Korppi-Tommola J. Quantum chemical simuation of excited states of chlorophylls, bacteriochlorophylls and their complexes. Physical Chemistry Chemical Physics. 2006;**8**:663-687. DOI: 10.1039/B513086G

[35] Leiger K, Linnanto JM, Freiberg A. Establishment of the Q_y absorption spectrum of chlorophyll *a* extending to near-infrared. Molecules. 2020;**25**:3796. DOI: 10.3390/molecules25173796

[36] Rebane KK. Impurity Spectra of Solids. New York: Springer; 1970. DOI: 10.1007/978-1-4684-1776-0

[37] Linnanto J, Freiberg A, Korppi-Tommola J. Quantum chemical simulations of excited-state absorption spectra of photosynthetic bacterial reaction center and antenna complexes. The Journal of Physical Chemistry. B. 2011;**115**:5536-5544. DOI: 10.1021/jp111340w

[38] Razjivin A, Solov'ev A, Kompanets V, Chekalin S, Moskalenko A, Lokstein H. The origin of the "dark" absorption band near 675 nm in the purple bacteria core light-harvesting complex LH1: Two-photon measurements of LH1 and its subunit B820. Photosynthesis Research. 2019; **140**:207-213. DOI: 10.1007/s11120-018-0602-0

[39] Bowers PG, Porter FRS. Quantum yields of triplet formation in solutions of chlorophyll. Proceedings of the Royal Society of London A. 1967;**296**:435-441. DOI: 10.1098/rspa.1967.0036

[40] Takiff L, Boxer SG. Phosphorescence spectra of bacteriochlorophylls. Journal of the American Chemical Society. 1988;**110**: 4425-4426. DOI: 10.1021/ja00221a059

[41] Neverov KV, Santabarbara S, Krasnovsky AAJ. Phosphorescence study of chlorophyll *d* photophysics. Determination of the energy and lifetime

of the photo-excited triplet state. Evidence of singlet oxygen photosensitization. Photosynthesis Research. 2011;**108**:101-106. DOI: 10.1007/s11120-011-9657-x

[42] Musewald C, Hartwich G, Pöllinger-Dammer F, Lossau H, Scheer H, Michel-Beyerle ME. Time-resolved spectral investigation of bacteriochlorophyll *a* and its transmetalated derivatives [Zn]-bacteriochlorophyll *a* and [Pd]-bacteriochlorophyll *a*. The Journal of Physical Chemistry. B. 1998;**102**: 8336-8342. DOI: 10.1021/jp982309z

[43] Teuchner K, Stiel H, Leupold D, Scherz A, Noy D, Simonin I, et al. Fluorescence and excited state absorption in modified pigments of bacterial photosynthesis a comparative study of metal-substituted bacteriochlorophylls *a*. Journal of Luminescence. 1997;**72-74**:612-614. DOI: 10.1016/S0022-2313(96)00411-5

[44] Davydov AS. Theory of Molecular Excitons. New York: Plenum Press; 1971. ISBN: 0306304406978030630440 8

[45] Shipman LL, Norris JR, Katz JJ. Quantum mechanical formalism for computation of the electronic spectral properties of chlorophyll aggregates. The Journal of Physical Chemistry. 1976;**80**: 877-882. DOI: 10.1021/j100549a023

[46] Linnanto J, Helenius VM, Oksanen JAI, Peltola T, Garaud J-L, Korppi-Tommola JEI. Exciton interactions and femtosecond relaxation in chlorophyll *a*—water and chlorophyll *a*—dioxane aggregates. The Journal of Physical Chemistry. A. 1998;**102**: 4337-4349. DOI: 10.1021/jp9728520

[47] Gouterman M. Spectra of porphyrins. Journal of Molecular Spectroscopy. 1961;**6**:138-163. DOI: 10.1016/0022-2852(61)90236-3

[48] Gouterman M, Wagnière GH, Snyder LC. Spectra of porphyrins: Part II. Four orbital model. Journal of Molecular Spectroscopy. 1963;**11**: 108-127. DOI: 10.1016/0022-2852(63)90011-0

[49] Saito K, Mitsuhashi K, Ishikita H. Dependence of te chlorophyll wavelength on the orientation of a charged group: Why does the accessory chlorophyll have a low site energy in photosystem II? Journal of Photochemical and Photobiology A. 2020;**402**:112799. DOI: 10.1016/j.jphotochem.2020.112799

[50] Linnanto J, Korppi-Tommola J. Spectroscopic properties of Mg-chlorin, Mg-porphin and chlorophylls *a, b,* c_1, c_2, c_3 and *d* studied by semi-empirical and *ab initio* MO/CI methods. Physical Chemistry Chemical Physics. 2000;**2**: 4962-4970. DOI: 10.1039/B004998K

[51] Linnanto J, Korppi-Tommola J. Spectroscopic properties of Mg-chlorin, Mg-bacteriochlorin, and bacteriochlorophylls *a, b, c, d, e, f, g,* and *h* studied by semiempirical and ab initio MO/CI methods. The Journal of Physical Chemistry. A. 2001;**105**:3855-3866. DOI: 10.1021/jp0021547

[52] Linnanto J, Korppi-Tommola J. Semiempirical PM5 molecular orbital study on chlorophylls and bacteriochlorophylls: Comparison of semiempirical, *ab initio*, and density functional results. Journal of Computational Chemistry. 2004;**25**: 123-137. DOI: 10.1002/jcc.10344

[53] Petke JD, Maggiora GM, Shipman LL, Christoffersen RE. Stereoelectronic properties of photosynthetic and related systems-VI. Ab initio configuration interaction calculations on the ground and lowest excited singlet and triplet states of ethyl

bacteriochlorophyllide-*a* and ethyl bacteriopheophorbide-*a*. Photochemistry and Photobiology. 1980; **32**:399-414. DOI: 10.1111/j.1751-1097.1980.tb03780.x

[54] Petke JD, Maggiora GM, Shipman L, Christoffersen RE. Stereoelectronic properties of photosynthetic and related systems-V. *Ab initio* configuration interaction calculations on the ground and lower excited singlet and triplet states of ethyl chlorophyllide *a* and ethyl pheophorbide *a*. Photochemistry and Photobiology. 1979;**30**:203-223. DOI: 10.1111/j.1751-1097.1979.tb07138.x

[55] Haran G, Wynne K, Moser CC, Dutton PL, Hochstrasser RM. Level mixing and energy redistribution in bacterial photosynthetic reaction centers. The Journal of Physical Chemistry. 1996;**100**:5562-5569. DOI: 10.1021/jp952925k

[56] Palm DM, Agostini A, Averesch V, Girr P, Werwie M, Takahashi S, et al. Chlorophyll *a/b* binding-specificity in water-soluble chlorophyll protein. Nature Plants. 2018;**4**:920-929. DOI: 10.1038/s41477-018-0273-z

[57] Fresch E, Meneghin E, Agostini A, Paulsen H, Carbonera D, Collini E. How the protein environment can tune the energy, the coupling, and the ultrafast dynamics of interacting chlorophylls: The example of the water-soluble chlorophyll protein. Journal of Physical Chemistry Letters. 2020;**11**:1059-1067. DOI: 10.1021/acs.jpclett.9b03628

[58] Linnanto J, Korppi-Tommola JEI, Helenius VM. Electronic states, absorption spectrum and circular dichroism spectrum of the photosynthetic bacterial LH2 Antenna of *Rhodopseudomonas acidophila* as predicted by exciton theory and semiempirical calculations. The Journal of Physical Chemistry. B. 1999;**103**: 8739-8750. DOI: 10.1021/jp9848344

[59] Linnanto J, Korppi-Tommola JEI. Theoretical study of excitation transfer from modified B800 rings of the LH II antenna complex of *Rps. acidophila*. Physical Chemistry Chemical Physics. 2002;**4**:3453-3460. DOI: 10.1039/B108338B

[60] McLuskey K, Prince SM, Cogdell RJ, Isaacs NW. The crystallographic structure of the B800-820 LH3 light-harvesting complex from the purple bacteria *Rhodopseudomonas acidophila* strain 7050. The Biochemist. 2001;**40**: 8783-8789. DOI: 10.1021/bi010309a

[61] McDermott G, Prince SM, Freer AA, Hawthornthwaite-Lawless AM, Papiz MZ, Cogdell RJ, et al. Crystal structure of an integral membrane light-harvesting complex from photosynthetic bacteria. Nature. 1995;**374**:517-521. DOI: 10.1038/374517a0

[62] Freiberg A, Timpmann K, Trinkunas G. Spectral fine-tuning in excitonically coupled cyclic photosynthetic antennas. Chemical Physics Letters. 2010;**500**:111-115. DOI: 10.1016/j.cplett.2010.09.084

[63] Yu L-J, Kawakami T, Kimura Y, Wang-Otomo Z-Y. Structural basis for the unusual Q_y red-shift and enhanced thermostability of the LH1 complex from *Thermochromatium tepidum*. The Biochemist. 2016;**55**:6495-6504. DOI: 10.1021/acs.biochem.6b00742

[64] Yu L-J, Suga M, Wang-Otomo Z-Y, Shen J-R. Structure of photosynthetic LH1-RC supercomplex at 1.9 Å resolution. Nature. 2018;**556**:209-214. DOI: 10.1038/s41586-018-0002-9

[65] Fowler GJS, Sockalingum GD, Robert B, Hunter CN. Blue shifts in

bacteriochlorophyll absorbance correlate with changed hydrogen bonding patterns in light-harvesting 2 mutants of Rhodobacter sphaeroides with alterations at α-Tyr-44 and α-Tyr-45. The Biochemical Journal. 1994;**299**: 695-700. DOI: 10.1042/bj2990695

[66] Wellman SMJ, Jockusch RA. Tuning the intrinsic photophysical properties of chlorophyll *a*. Chemistry: A European Journal. 2017;**23**:7728-7736. DOI: 10.1002/chem.201700349

[67] Milne BF, Toker Y, Rubio A, Nielsen SB. Unraveling the intrinsic color of chlorophyll. Angewandte Chemie, International Edition. 2015;**54**: 2170-2173. DOI: 10.1002/anie.201410899

[68] Gülen D. Significance of the excitonic intensity borrowing in the J-/H-aggregates of bacteriochlorophylls/chlorophylls. Photosynthesis Research. 2006;**87**:205-214. DOI: DOI/10.1007/s11120-005-8408-2

[69] Zucchelli G, Brogioli D, Casazza AP, Garlaschi FM, Jennings RC. Chlorophyll ring deformation modulates Q_y electronic energy in chlorophyll-protein complexes and generates spectral forms. Biophysical Journal. 2007;**93**:2240-2254. DOI: 10.1529/biophysj.107.104554

[70] Rätsep M, Linnanto J, Freiberg A. Mirror symmetry and vibrational structure in optical spectra of chlorophyll *a*. The Journal of Chemical Physics. 2009;**130**:194501. DOI: 10.1063/1.3125183

[71] Rätsep M, Linnanto JM, Freiberg A. Higher order vibronic sidebands of chlorophyll *a* and bacteriochlorophyll *a* for enhanced excitation energy transfer and light harvesting. The Journal of Physical Chemistry. B. 2019;**123**: 7149-7156. DOI: 10.1021/acs.jpcb.9b06843

[72] Song Y, Schubert A, Maret E, Burdick RK, Dunietz BD, Geva E, et al. Vibronic structure of photosynthetic pigments probed by polarized two-dimensional electronic spectroscopy and *ab initio* calculations. Chemical Science. 2019;**10**:8143-8153. DOI: 10.1039/c9sc02329a

[73] Rätsep M, Freiberg A. Electron-phonon and vibronic couplings in the FMO bacteriochlorophyll *a* antenna complex studied by difference fluorescence line narrowing. Journal of Luminescence. 2007;**127**:251-259. DOI: 10.1016/j.jlumin.2007.02.053

[74] Jankowiak R, Reppert M, Zazubovich V, Pieper J, Reinot T. Site selective and single complex laser-based spectroscopies: A window on excited state electronic structure, excitation energy transfer, and electron-phonon coupling of selected photosynthetic complexes. Chemical Reviews. 2011;**111**: 4546-4598. DOI: 10.1021/cr100234j

[75] Holt AS, Jacobs EE. Infra-red absorption spectra of chlorophylls and derivatives. Plant Physiology. 1955;**30**: 553-559. DOI: 10.1104/pp.30.6.553

[76] Leiger K, Linnanto JM, Freiberg A. Vibronic origin of the Q_y absorption tail of bacteriochlorophyll *a* verified by fluorescence excitation spectroscopy and quantum chemical simulations. Journal of Physical Chemistry Letters. 2017;**8**: 4231-4235. DOI: 10.1021/acs.jpclett.7b01704

[77] Reimers JR, Cai Z-L, Kobayashi R, Rätsep M, Freiberg A, Krausz E. Assignment of the Q-band of the chlorophylls: Coherence loss via $Q_x - Q_y$ mixing. Scientific Reports. 2013;**3**: 2761-2768. DOI: 10.1038/srep02761

[78] Rätsep M, Linnanto JM, Muru R, Biczysko M, Reimers JR, Freiberg A.

Absorption-emission symmetry breaking and the different origins of vibrational structures of the ^1Q_y and ^1Q_x electronic transitions of pheophytin *a*. The Journal of Chemical Physics. 2019;**151**:165102. DOI: 10.1063/1.5116265

[79] Linnanto JM, Korppi-Tommola JEI. Modelling excitonic energy transfer in the photosynthetic unit of purple bacteria. Chemical Physics. 2009;**357**: 171-180. DOI: 10.1016/j.chemphys.2009.01.001

[80] Pieper J, Rätsep M, Trostmann I, Paulsen H, Renger G, Freiberg A. Excitonic energy level structure and pigment-protein interactions in the recombinant water-soluble chlorophyll protein. I. Difference fluorescence line-narrowing. The Journal of Physical Chemistry. B. 2011;**115**:4042-4052. DOI: 10.1021/jp111455g

[81] Bednarczyk D, Dym O, Prabahar V, Peleg Y, Pike DH, Noy D. Fine tuning of chlorophyll spectra by pigment-induced ring deformation. Angewandte Chemie, International Edition. 2016;**55**: 6901-6905. DOI: 10.1002/anie.201512001